

# Free Surface Deformation of the Weld Pool in Orbital Narrow Groove GTA Welding

S. Morville<sup>1</sup>, V. Bruyere<sup>2</sup>, P. Namy<sup>2</sup>

1. Technical Center FRAMATOME, 30 Boulevard de l'Industrie, 71200 Le Creusot, France

2. SIMTEC, 155 Cours Berriat, 38000 Grenoble, France

## 1. Introduction

Arc welding is a widespread process in heavy industry for the assembly of metallic components. In order to ensure the good quality of welded assemblies, it is appropriate to master the welding process but also to have a deep understanding of interactions within the weld pool and resulting characteristics of the weld.

The objective of this work is to develop an accurate model able to predict the dimensions of the melted zone and the weld seam under several operating conditions. Numerical simulation is used here as a predictive *in situ* analysis tool which provides additional data to real-time measurements. Therefore, it requires to take into account main physical phenomena such as heat transfer, fluid flow inside the weld pool, and also electromagnetic phenomena induced by the electrical arc and the deformation of the top surface. While in some studies in the literature the weld pool surface was considered flat and fixed, other approaches have been proposed to solve this kind of complex problem [1-5]. The development of a multi-physics model using Comsol Multiphysics® and its application to an industrial geometry are presented in this paper. After a short description of the main physical phenomena, a three-dimensional steady-state model is implemented with energy, momentum, mass and current conservation equations. Details concerning the equations and boundary conditions are provided. Due to strong nonlinearities and multi-physics phenomena, numerical aspects have to be carefully handled. The results obtained for classical operating conditions of welding are then presented and discussed. The influence of filler material and welding position on the weld bead is studied, highlighting the added value of numerical simulations.

## 2. Physical phenomena

Several physical phenomena have to be considered simultaneously to predict the melted area and welded joint shapes. Both resulting characteristics are crucial in welding studies and require a thorough

understanding of the physics phenomena involved throughout the process.

During arc welding, the electrical arc plasma transfers heat, current and momentum to the workpiece. The liquid metal flows due to surface and volume forces, then it affects the heat distribution inside the melt pool. Therefore the weld pool and solidified seam shapes are strongly affected by welding configuration, defined by: the welding parameters, the materials, the workpiece geometry and the welding position. In particular, the free surface of the melt pool is stretched because of surface forces (arc pressure, surface tension) and filler material. The gravity forces also need to be included in the model as it will influence the shape of the weld seam given the welding position. Momentum and energy of the filler metal combined with shear stresses induced by the plasma flow should also be considered. While the electrical arc plasma and the filler wire are not modelled explicitly, an equivalent approach is used to simulate these contributions. It is enough to have an almost self-consistent model able to highlight the mains trends of the welding processes. The benefit of such model is that the melt pool and the weld bead characteristics are numerical results based on physical phenomena, instead of an arbitrary assumption.

Here the model capabilities are shown through a standard welding application, which is the filling sequence of a narrow groove with a GTA welding process as shown in **Figure 1**. Robustness of the process and behavior of the melt pool regarding the welding position will be discussed.

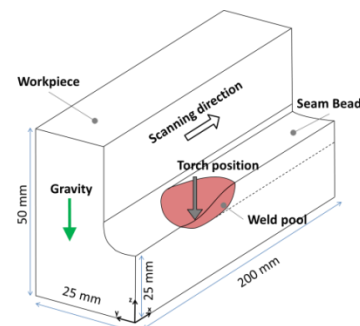


**Figure 1.** Sketch of the studied welding application – Filling sequence of a narrow groove

### 3. Governing Equations

The governing equations are written in the mobile frame of the welding torch and a stationary solver is used. It allows to decrease drastically the domain size and the computational time. Moreover, a perfect contact is considered between the two parts of the assembly (no berthing assumption), that allows to exploit the plane of longitudinal symmetry of the workpiece.

#### 3.1. Electromagnetic problem

The electromagnetic problem is governed by Maxwell's equations. The formulation in terms of magnetic potential vector  $\mathbf{A}$  is used in Comsol Multiphysics® with the current continuity equation. It is expressed by the following equations:

$$\nabla \times \left( \frac{1}{\mu_0} \nabla \times \mathbf{A} \right) + \sigma \nabla V = 0 \quad (1)$$

$$\nabla \cdot (\sigma \nabla V) = 0 \quad (2)$$

where  $\mu_R$  is the relative permeability,  $\sigma$  is the electrical conductivity and  $V$  is the electric potential.

The magnetic flux density,  $\mathbf{B}$ , the current density,  $\mathbf{J}$ , and the electric field,  $\mathbf{E}$ , are obtained with the following relations:

$$\mathbf{B} = \nabla \times \mathbf{A} \quad (3)$$

$$\mathbf{J} = -\sigma \nabla V \quad (4)$$

$$\mathbf{E} = -\nabla V \quad (5)$$

Concerning the boundary conditions, the current density from the arc plasma is assumed to be Gaussian at the top surface:

$$-\mathbf{n} \cdot \mathbf{J} = d \frac{I_0}{\pi r_{elec}^2} e^{\left( -d \frac{((x-x_t)^2 + y^2)}{r_{elec}^2} \right)} \quad (6)$$

where  $d$  is a distribution coefficient,  $I_0$  is the nominal intensity,  $r_{elec}$  is the radius of the electrical source and  $x_t$  is the x-position of the welding torch. A reference potential ( $V = 0$ ) is applied at the lower surface. Other boundaries are isolated. Lastly, due to electromagnetic interactions, two bulk sources and couplings are generated:

- a heat source term due to resistive loss (Joule effect):  $Q_{EM} = \frac{1}{2} \text{Re}(\mathbf{J} \cdot \mathbf{E}^*)$

- a body force affecting the fluid flow (Lorentz Force) expressed by:

$$\mathbf{F}_{EM} = \mathbf{J} \times \mathbf{B}$$

#### 3.2. Thermal problem

In order to obtain the temperature distribution, the heat equation is solved in its classical convection/diffusion form:

$$\rho C_p (\mathbf{u} - \mathbf{u}_{weld}) \cdot \nabla T = \nabla \cdot (k \nabla T) + Q_{EM} \quad (7)$$

where  $\rho$  is the density,  $C_p$  is the heat capacity,  $k$  is the conductivity,  $T$  is the temperature.  $\mathbf{u}_{weld}$  and  $\mathbf{u}$  are the welding velocity and the fluid velocity vectors, respectively. The latent heat of fusion/solidification is included in the  $C_p$  variable *via* the use of the apparent heat capacity method based on liquid fraction variation as shown in [3]. It should be noted that the thermal impact of the filler metal is not implemented in the present work. Ambient conditions are taken into account by describing convective and radiation transfers at the upper and lower surfaces, as well as the heat flux from the arc (assumed to be Gaussian) and the liquid metal evaporation:

$$-\mathbf{n} \cdot (-k \nabla T) = d \frac{\eta U_0 I_0}{\pi r_{heat}^2} e^{\left( -d \frac{((x-x_t)^2 + y^2)}{r_{heat}^2} \right)} - Q_{vap} + h_c (T_{ext} - T) + \varepsilon \sigma (T_{ext}^4 - T^4) \quad (8)$$

$$Q_{vap} = p_{ext} \exp \left[ \frac{M_v H_v}{R_0} \left( \frac{1}{T_v} - \frac{1}{T} \right) \right] \sqrt{\frac{M_v}{2\pi R_0 T}} (1 - \beta_r) H_v \quad (9)$$

where  $h_c$  is the convective heat transfer coefficient,  $T_{ext}$  is the ambient temperature,  $\varepsilon$  is the surface emissivity,  $\sigma$  is the Stefan-Boltzmann constant,  $U_0$  is the nominal voltage,  $\eta$  is the thermal efficiency of the welding process and  $r_{heat}$  is the radius of the thermal source.  $p_{ext}$  is the external absolute pressure,  $M_v$  is the molar weight of metallic vapors,  $H_v$  is the latent heat of vaporization,  $T_v$  is the vaporization temperature,  $R_0$  is the ideal gas constant and  $\beta_r$  is the retro-diffusion coefficient. Due to the mobile frame formulation, a temperature  $T_{ext}$  and a zero heat flux are defined at the upstream and downstream boundary conditions, respectively. Other boundaries are assumed to be isolated.

### 3.3. Fluid Mechanics

Subjected to different forces (arc pressure, capillary effects, gravity, electromagnetic forces), the molten metal flows. By considering an incompressible flow and the liquid metal as a Newtonian fluid, the following equations are solved to compute the velocities and pressure fields:

$$\nabla \cdot (\mathbf{u}) = 0 \quad (10)$$

$$\rho_L (\mathbf{u} \cdot \nabla) \mathbf{u} = \nabla \cdot \left( -p\mathbf{I} + \mu(\nabla \mathbf{u} + (\nabla \mathbf{u})^T) \right) + \mathbf{F}_{\text{Darcy}} + \mathbf{F}_{\text{EM}} + \mathbf{F}_{\text{Buoyancy}} \quad (11)$$

$$\mathbf{F}_{\text{Darcy}} = -C \left( \frac{(1-f_l)}{f_l^3 + b} \right) (\mathbf{u} - \mathbf{u}_{\text{weld}}) \quad (12)$$

$$\mathbf{F}_{\text{Buoyancy}} = -\rho_L \beta_L (T - T_m) \mathbf{g} \quad (13)$$

where  $\mathbf{u}$  is the fluid velocities vector,  $p$  is the pressure,  $\mu$  is the dynamic viscosity and  $\rho_L$  is the metal density at  $T_L$ . A volum force  $\mathbf{F}_{\text{Darcy}}$  is added in equation (10) as proposed in [6] to treat the phase change. Then the solid phase is assumed to behave as a fluid with an infinite stiffness.  $C$  and  $b$  are constants and  $f_l$  is the liquid fraction going from 0 to 1 between  $T_s$  and  $T_L$ , the solidus and liquidus temperatures, respectively.  $\mathbf{F}_{\text{Buoyancy}}$  includes the contribution of density variations due to the temperature; the Boussinesq assumption is used to deal with the incompressible formulation of the fluid mechanics problem.  $\beta_L$  is the thermal expansion coefficient,  $T_m$  the melting temperature ( $T_m = \frac{T_s + T_L}{2}$ ) and  $\mathbf{g}$  is the gravity vector. Due to the low dynamic of the metallic transfer, momentum of droplets is not included here. Shear stresses of the plasma flow are neglected too.

### 3.4. Free surface equation

As introduced previously, the free surface deformation is the result of several factors and highly influences the shape of the welded seam. A variational approach minimizing the total energy of the melt pool surface with an incompressibility constraint including the filler material mass flow is used. Details concerning this approach can be found in [7]. The resulting governing equation for the free surface shape is given by:

$$-\nabla \cdot \left( \frac{\gamma}{\sqrt{1 + \phi_x^2 + \phi_y^2}} \nabla \phi \right) = f \quad (14)$$

$\gamma$  is the surface tension coefficient depending on temperature and sulfur content  $a_s$  [8],  $\phi$  represents the vertical displacement of the melt pool surface, and  $f$  is the source term defined as:

$$f = P_{\text{arc}} + \rho g + \lambda \quad (15)$$

$$P_{\text{arc}} = d \frac{\mu_0 I_0^2}{4\pi^2 r_{\text{arc}}^2} e^{\left( -d \frac{(x-x_c)^2 + y^2}{r_{\text{arc}}^2} \right)} \quad (16)$$

where  $P_{\text{arc}}$  is the arc pressure distribution,  $g$  is the gravity constant and  $\lambda$  is a Lagrange multiplier,  $\mu_0$  is the vacuum permeability and  $r_{\text{arc}}$  is the radius of the loading source. Boundary conditions are the follows:

- at the front pool:  $\phi = 0$
- at the rear pool:  $\frac{\partial \phi}{\partial x} = 0$ ,

Since the deposited area at a solidified cross section of the fillet weld is equal to the amount of fed wire per unit length, the constraining equation is given as:

$$\int \phi dy = \frac{\pi r_{\text{wire}}^2 V_{\text{wire}}}{V_{\text{weld}}} \quad (17)$$

where  $r_{\text{wire}}$  is the wire radius and  $V_{\text{wire}}$  the wire velocity. An extra ODE (17) is thus added to the problem. It is linked to the whole system of equations by the Lagrange multiplier  $\lambda$ , associated to the free surface equation (14).

### 3.5. Moving Mesh

Lastly, an ALE approach is used to move the nodes according to the free surface deformation. The hyperelastic method is used, by solving the following potential:

$$W = \int_{\Omega} \frac{\eta}{2} (I_1 - 3) + \frac{\kappa}{2} (J - 1)^2 dV \quad (18)$$

where  $\eta$  and  $\kappa$  are artificial shear and bulk moduli respectively and the invariants  $J$  and  $I_1$  are given by:

$$J = \det(\nabla_{\mathbf{x}} \mathbf{x}) \quad (19)$$

$$I_1 = J^{-\frac{2}{3}} \text{tr}((\nabla_{\mathbf{x}} \mathbf{x})^T \nabla_{\mathbf{x}} \mathbf{x}) \quad (20)$$

Displacements of the nodes at the top surface are driven by the following relation:  $z - Z = \phi$ . Other mesh displacements are constrained in all directions apart from those in the symmetry plane which are free to move in the  $z$ -direction.

All these equations are needed to predict accurately the shape of the melted joint. However, they are strongly coupled and some of them amplify sharp non-linearities. To reach convergence to the stationary state of the whole problem, careful and specific considerations with regards to numerical aspects are required.

#### 4. Numerical Aspects

Sharp gradients are encountered in welding, inter alia, because of the high density of the thermal source and the specificity of the flow pattern. Consequently, the mesh has to be carefully built to ensure the validity of the numerical results. The mesh used in this work is shown in **Figure 2**. The average elements size is 150  $\mu\text{m}$  in domain  $\Omega_2$  and coarser elements are used in others domains ( $\Omega_1$  and  $\Omega_3$ ).

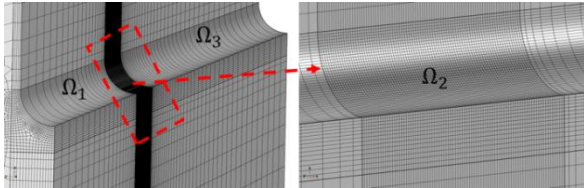


**Figure 2.** Extruded and regular mesh

To obtain the numerical convergence for this highly coupled problem, unknown variables are computed with segregated steps and the MUMPS direct solver. Each step is customized (damping coefficient, number of iteration) to reach a steady-state solution. The CPU time needed to solve the 1,009,934 degrees of freedom is roughly 10 hours with 6 cores and 192 Go RAM.

#### 5. Welding application

The application example presented in this paper is the deposition of a single bead at mid-depth of a narrow groove. Base material and filler material are identical and made of 316L stainless steel with thermal-dependent physical properties [9]. Constant parameters are given in the following table:

$\beta_L$ [1/K]	$1.89 \times 10^{-4}$	$I_0$ [A]	200
$\beta_r$ [-]	0.5	$M_v$ [g/mol]	56
$\varepsilon$ [1]	0.4	$p_{\text{ext}}$ [Pa]	$10^5$
$\eta$ [1]	0.7	$r_{\text{arc}}$ [m]	$3 \times 10^{-3}$
$\rho_L$ [kg/m <sup>3</sup> ]	6500	$r_{\text{elec}}$ [m]	$3 \times 10^{-3}$
$\mu_r$ [1]	1	$r_{\text{heat}}$ [m]	$3 \times 10^{-3}$
$a_S$ [%]	0.01	$r_{\text{wire}}$ [m]	$5 \times 10^{-4}$
$b$ [1]	$10^{-3}$	$T_{\text{ext}}$ [K]	293
$C$ [kg/s/m <sup>3</sup> ]	$10^9$	$T_L$ [K]	1723
$d$ [1]	3	$T_S$ [K]	1663
$h_c$ [W/m <sup>2</sup> /K]	20	$T_v$ [K]	3200

$H_m$ [J/kg]	$2.5 \times 10^5$	$u_{\text{weld}}$ [m/s]	$2 \times 10^{-3}$
$H_v$ [J/kg]	$6 \times 10^6$	$u_{\text{wire}}$ [m/s]	$16 \times 10^{-3}$

**Table 1.** Values of constant parameters used in computations

The welding position is also a parameter of interest. Studied positions and their designation are the following: flat position 1G, up vertical position 3GU and down vertical position 3GD. The overhead position 4G is not studied here.

#### 6. Simulation Results

Several factors influence the melted zone and the welded joint dimensions. Numerical modeling is an appropriate tool to evaluate the influence of each of them. To reach a better understanding of the process and further inform the monitoring of the process, the influence of the filler metal and the welding position are studied.

##### 6.1. Influence of the filler metal

A comparison is performed between an arbitrary case without filler material and a nominal case with filler material (a flat welding position is assumed). A narrow groove welding configuration is studied here.

In **Figure 3**, the steady-state fields of temperature and velocities are presented. The white lines are isothermal levels and the thick line is the melting temperature  $T_m$ . Some characteristics of the melt pool are given in **Table 2**. The shape of the melt pool is mainly affected by the metal flow and two distinct areas can be observed. The first one is just near the arc plasma and experiences high surface temperatures going from 2200 K to 2769 K with an averaged velocity of 0.3 m/s. The second one is in the back with lower temperatures (1800 K) and velocities (0.15 m/s). Such situation is well-known and caused by the Marangoni effect, with opposing directions of the shear stresses regarding the temperature level. It leads to the appearance of convective cells with contrary rotation making the melt pool deeper at the rear than under the welding torch. Hence the pool depth is decreased which reduces the effect of the volume forces (Lorentz and Buoyancy) on the flow. Then, the depression of the free surface is mainly induced by the arc plasma pressure.

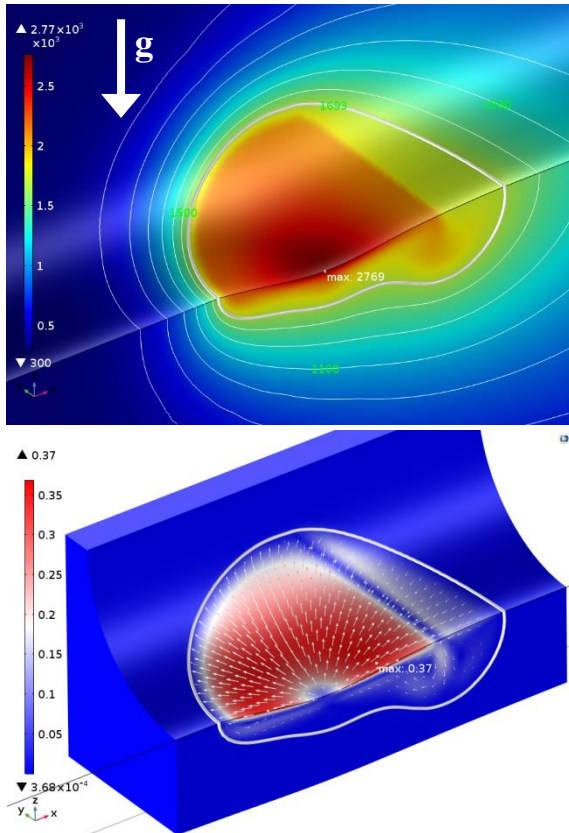


**Figure 3.** Temperature and velocity fields in the melt pool without filler material (1G position)

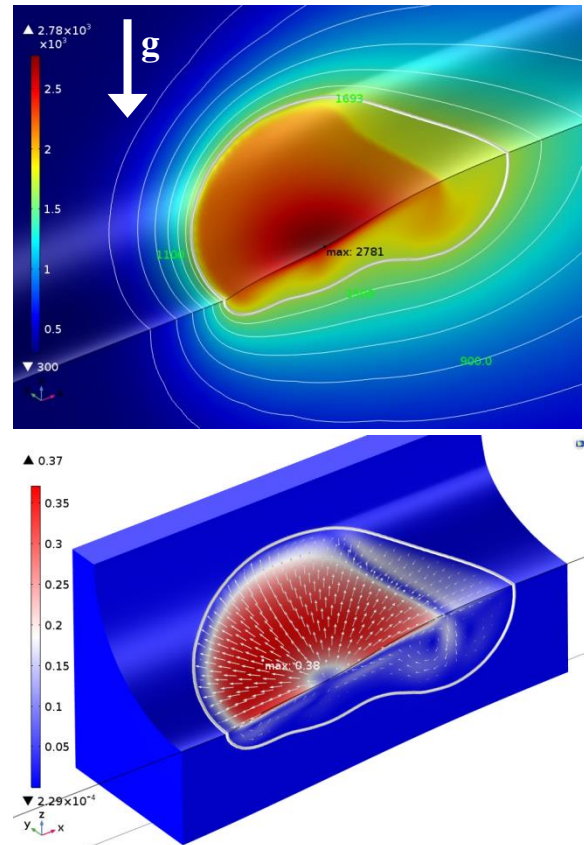


**Figure 4.** Temperature and velocity fields in the melt pool with filler material (1G position)

The results of the computation with filler metal are presented in **Figure 4**. It can be seen from **Figure 4** that the results obtained from the simulation involving the filler metal are similar to those with no filler metal, presented in **Figure 3**. However, it should be noted that the simulation leads to a 1.2 mm bead height, compared to zero height in the previous case (see **Figure 5**). This z-displacement is due to the incompressibility constraint (17). As a consequence the penetration depth decreases while the melt pool thickness and the melt pool volume remain the same.

Specific characteristics of each melt pool are given in **Table 2** in order to have some orders of magnitude regarding dimensions, melted volume, maximum / averaged temperature and velocities. Apart from the penetration depth and the bead height, the adding material effects have little impacts.

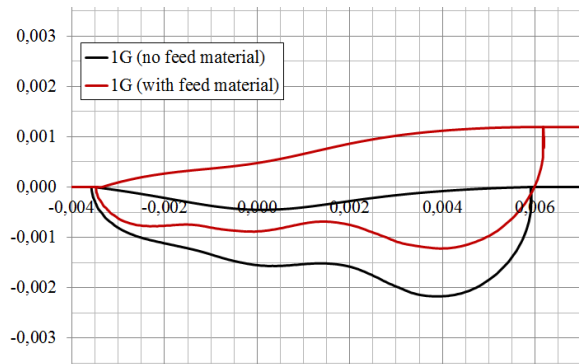


**Figure 5.** Cross-sectional view of the melt pool along the xz plane depending on the feed rate conditions in 1G welding position

## 6.2. Influence of the welding position

The rotation of the welding torch inside the narrow groove makes the weld pool sensitive to the gravity field. Particular attention is paid to variations of the pool. In **Figure 6** the temperature field of the workpiece is presented in up vertical and down vertical positions, 3GU and 3GD respectively. While the free surface is not significantly affected by the hydrostatic pressure change, main characteristics of

the pool are unaltered (**Table 2**). This can be observed in **Figure 7** where the comparison of the pool shapes in 1G, 3GU and 3GD positions shows little difference. Whereas the 1G and 3GD positions have very similar shapes, the 3GU position shows a larger deformation at the back of the pool, which is an effect of the heavy liquid metal. The front of the pool is constrained by the arc plasma pressure and shows a moderated sensitivity to the welding position.

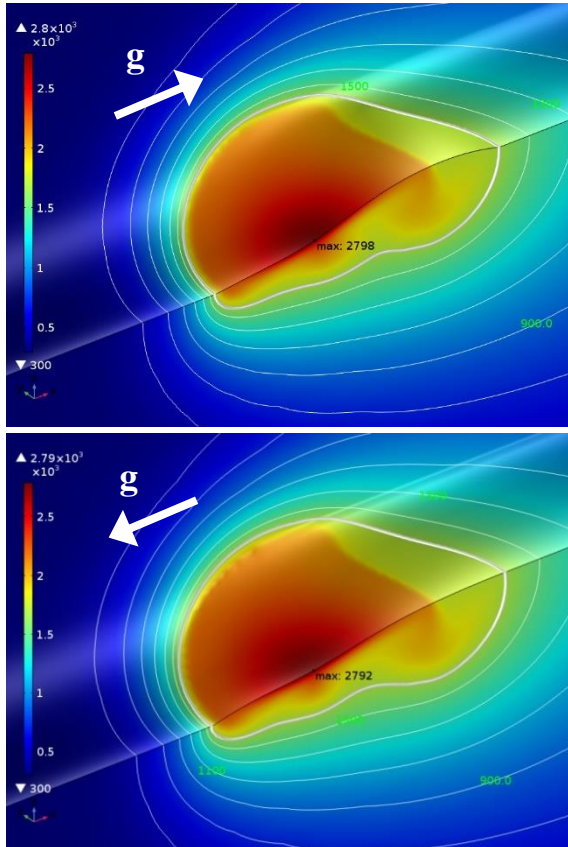


**Figure 6.** Temperature field in the melt pool with filler material in different welding positions (up = 3GU, down = 3GD)

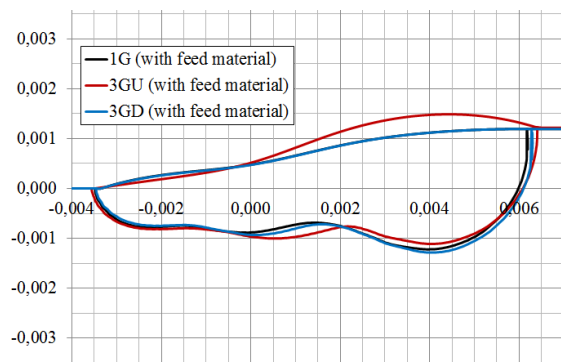


**Figure 7.** Cross-sectional view of the melt pool along the xz plane depending on the welding position

	No filling	With filling		
	(1G)	(1G)	(3GU)	(3GD)
L [mm]	9.5	9.6	9.9	9.7
W [mm]*	8.2	8.2	8.4	8.4
D [mm]	2.2	1.2	1.2	1.3
h[mm]	0	1.2	1.2	1.2
$V_{pool}$ [mm <sup>3</sup> ]*	93.4	96.6	103.6	99.4
$T_{max}$ [K]	2796	2781	2798	2792
$T_{ave}$ [K]	2142	2153	2152	2153
$U_{max}$ [m/s]	0.37	0.38	0.38	0.38
$U_{ave}$ [m/s]	0.22	0.23	0.23	0.23

**Table 2.** Characteristics of the computed melt pools: length L, width W, depth D, bead height h, melt pool volume  $V_{pool}$ , maximal and averaged temperature and velocities at the pool surface

The simulated pool behaviors presented in this paper are in good agreement with the state-of-art of the GTA welding knowledge and builds up confidence in the model capabilities to predict trends of welding processes. However, precautions need to be taken about current results. Firstly, the arc plasma / weld pool interactions must be handled to deal with the effects of surface deformations on the plasma distributions (heat, momentum, current). Secondly, the use of artificial inputs with Gaussian distribution involves standard deviations that are arbitrary defined here. Such values are very complex to identify because of a high dependency to the welding gas and the electrode design. Lastly, the steady-state approach involves to smooth some parameters. Consequently, dynamic phenomena like the arc current pulsation or the torch sweeping are ignored. Future developments shall be performed to enhance and generalize the present physical model.

## 7. Conclusions

A three-dimensional multiphysics model has been developed to predict the dimensions of the weld pool and seam bead, by considering different physical phenomena. Due to sharp non-linearities and strong couplings, numerical aspects have been carefully managed to maintain convergence.

After numerical validations on a reference case, the influence of the filler material and the welding position has been studied based on an industrial geometry, i.e. the orbital GTA welding in narrow groove. Results show the influence of the filler material on the weld pool penetration and dilution. Whereas it doesn't seem to impact the thermal and flow fields, it must be noticed that the energetic and mechanical contributions of filler metal are not taken into account yet. Furthermore, it has been shown that

the melt pool has very few sensitivity to the gravity field variations, that is in good agreement with the state-of-the-art. Early results are promising and shall be strengthened by a comparison between model outputs and experimental data from dedicated and instrumented mockups.

## 8. References

1. Traidia et al., “On the effects of gravity and sulfur content on the weld shape in horizontal narrow gap GTAW of stainless steel”, *Journal of Materials Processing Technology* 213, 1128-1138 (2013)
2. Kim et al., Modeling of temperature field and solidified surface profile during gas-metal arc fillet welding, *Journal of Applied Physics*, **95**, 4, 2667-2678 (2003)
3. Le Guen et al., 3D heat transfer model of hybrid laser Nd:Yag-MAG welding of S355 steel and experimental validation, *International Journal of Heat and Mass Transfer*, **54**, 1313-1322 (2011)
4. Xu et al., Characteristics and mechanisms of weld formation during oscillating arc narrow gap vertical up GMA welding, *Welding in the world*, **61**, 241-248, (2017)
5. Lu et al., Modeling and finite element analysis on GTAW arc and weld pool, *Computational Materials Science*, **29**, 371-378, (2004)
6. Beckermann et al., Double-Diffusive Convection during Dendritic Solidification of a Binary Mixture, *PhysicoChemical Hydrodynamics*, **10**, 195-213, (1988)
7. Wu et al., Numerical analysis of both front-and back-side deformation of fully penetrated GTAW weld pool surfaces, *Computational Materials Science*, **39**, 635-642 (2007)
8. Sahoo et al., “Surface tension of binary metal – Surface active solute systems under conditions relevant to welding metallurgy”, *Met. Trans. B*, Volume 19B (1998)
9. IAEA report, “Thermophysical properties of materials for nuclear engineering: a tutorial and collection of data” (2008)